Average and local structure of the Pb-free ferroelectric perovskites (Sr,Sn)TiO_{3} and (Ba,Ca,Sn)TiO_{3}

Geneva Laurita, Katharine Page, Shoichiro Suzuki, and Ram Seshadri

Average and local structure of the Pb-free ferroelectric perovskites $(Sr,Sn)TiO_3$ and $(Ba,Ca,Sn)TiO_3$

Geneva Laurita[*]

Materials Research Laboratory, University of California, Santa Barbara, CA 93106

Katharine Page

Chemical and Engineering Materials Division, Oak Ridge National Laboratory, Oak Ridge, TN 37831

Shoichiro Suzuki

Murata Manufacturing, Co., Ltd., Nagaokakyo, Kyoto 617-8555, Japan

Ram Seshadri

Materials Department and Materials Research Laboratory,
University of California, Santa Barbara, CA 93106

The characteristic structural off-centering of Pb^{2+} in oxides, associated with its $6s^2$ lone pair, allows it to play a dominant role in polar materials, and makes it a somewhat ubiquitous component of ferroelectrics. In this work, we examine the compounds $Sr_{0.9}Sn_{0.1}TiO_3$ and $Ba_{0.79}Ca_{0.16}Sn_{0.05}TiO_3$ using neutron total scattering techniques with data acquired at different temperatures. In these compounds, previously reported as ferroelectrics, Sn^{2+} appears to display some of the characteristics of Pb^{2+}. We compare the local and long-range structures of the Sn^{2+}-substituted compositions to the unsubstituted parent compounds $SrTiO_3$ and $BaTiO_3$. We find that even at these small substitution levels, the Sn^{2+} lone pairs drive the local ordering behavior, with the local structure of both compounds more similar to the structure of $PbTiO_3$ rather than the parent compounds.

I.   INTRODUCTION

The perovskite oxides ABO_3 form a class of highly-studied and technologically relevant materials, with many exhibiting ferroelectric behavior.[1] Of the ferroelectric perovskites, examples include $BaTiO_3$ and $PbTiO_3$, where the ferroelectric polarization is associated with the off-centering of Ti in TiO_6 octahedra due to so-called second-order Jahn-Teller effects.[2] In $PbTiO_3$, the Pb^{2+} ions on the A site additionally drive off-centering, due to the characteristic $6s^2$ lone pair.[3,4] The off-centerings can cooperatively give rise to spontaneous polarization and ferroelectric behavior. First principles studies have suggested that $SnTiO_3$ should similarly display off-centering due to the Sn^{2+} $5s^2$ lone pair, and this as yet experimentally unrealized compound is expected to exhibit a larger polarization than $PbTiO_3$.[5,6] This is in keeping with expected trends in lone-pair behavior of divalent carbon group compounds.[3] The environmentally benign nature of Sn^{2+} would make $SnTiO_3$-derived compounds an attractive alternative to Pb-containing ferroelectrics.

$SrTiO_3$ is an incipient ferroelectric that does not exhibit a ferroelectric transition above 0 K due to quantum fluctuations.[7] However, substitution of Sn^{2+} into the Sr^{2+} site of $SrTiO_3$ induces a relaxor-like ferroelectric transition.[8,9] Raman spectroscopic observations of polar transverse optic modes at room temperature suggest the ferroelectric behavior arises due to the formation of percolative polar nanoregions formed in the material.[10] A maximum dielectric permittivity was observed with a nominal 10 % Sn-substitution, and is therefore the composition chosen for this study.[8] In contrast to $SrTiO_3$,

$BaTiO_3$ is a room-temperature ferroelectric material that is commonly employed in multilayer ceramic capacitors. However, a relatively low ferroelectric transition temperature, T_c, of approximately 400 K limits the use of this material.[11] Efforts to increase the T_c of $BaTiO_3$ have been facilitated through the substitution of Pb^{2+} into the Ba^{2+} site,[12] but the toxicity of Pb leaves room for improvement for technological applications. To increase the solubility of the smaller Sn^{2+} into the lattice of $BaTiO_3$, the lattice volume can be decreased by the addition of Ca^{2+} into the A-site. It has been shown in the literature that the T_c of $(Ba,Ca)TiO_3$ remains relatively constant up to the solubility limit of Ca^{2+} (approximately 20 %), making this an accessible system to study the effects of Sn^{2+} substitution.[13,14] Successful Sn^{2+} substitution into perovskite titanates has been completed through the co-substitution of Ca^{2+} and Sn^{2+} into the Ba^{2+} site of $BaTiO_3$ and exhibits an increase of 20 K in the T_c for the nominal composition $Ba_{0.79}Ca_{0.16}Sn_{0.05}TiO_3$ (further studied here) compared to that of the unsubstituted compound.[15–18]

The presence of the lone pair of electrons bound to Sn^{2+} can induce off-centering, and since these off-centerings need not be correlated, it is necessary to utilize a structural technique that will analyze not only the average crystallographic structure but also the local structure in a material. This can be accomplished through the application of total scattering techniques, which utilize both the Bragg and diffuse components to provide information on the average structure (obtained from Rietveld refinement of the Bragg scattering) and the local structure (obtained from the real-space pair distribution function).

In particular, neutron scattering plays a crucial role in the structural analysis of oxide materials since scattering from oxygen contributes significantly to the total signal. There are numerous illustrations in the literature that the local structure of titanate perovskites frequently does not reflect the average crystallographic structure. For example, it has been observed that the local symmetry of the paraelectric phases in $BaTiO_3$ and $PbTiO_3$ is better described as the ferroelectric phases in space groups $R3m$[19] and $P4mm$[20] respectively. Similarly, Page et al.[21] have observed in Nb-substituted $BaTiO_3$, that the near-neighbor structure at all temperatures is reminiscent of the ferroelectric $R3m$ structure while the average structure is cubic $Pm\bar{3}m$ at all temperatures.

In this contribution, we investigate the local and average structure, using neutron total scattering methods, of two characteristic ferroelectric compounds with Sn^{2+}-substitution on the A-site of the perovskite structure $A^{2+}TiO_3$ (A^{2+} = Ba, Ca, Sr), using the compositions $Sr_{0.9}Sn_{0.1}TiO_3$ and $Ba_{0.79}Ca_{0.16}Sn_{0.05}TiO_3$. These compounds have been previously characterized from the viewpoint of their dielectric properties, Raman spectroscopy, average X-ray structure, and electron microscopy.[8,9,15–18] Some of the key findings that emerge include that despite the small substitution levels, the Sn^{2+} lone pairs drive the local ordering behavior. The local structure of both compounds more closely follow the behavior of $PbTiO_3$ than that of the parent compounds $SrTiO_3$ and $BaTiO_3$ respectively. This trend towards tetragonal symmetry below T_c upon substitution with Sn^{2+} is in agreement with recent DFT predictions.[22] Another surprising finding is that over very short length scales the Ti–O correlations in TiO_6 appear to become, somewhat counter-intuitively, more regular as the temperature is decreased. This effect appears to be more pronounced in $Sr_{0.9}Sn_{0.1}TiO_3$.

II. METHODS

Ceramic samples of nominal $Sr_{0.9}Sn_{0.1}TiO_3$ (SSTO) and $Ba_{0.79}Ca_{0.16}Sn_{0.05}TiO_3$ (BCSTO) were prepared through solid state routes and details are described elsewhere.[8,9,15–18] Time-of-flight (TOF) neutron scattering data was collected on powdered samples on the Nanoscale Ordered Materials Diffractometer (NOMAD) at the Spallation Neutron Source (SNS) located at Oak Ridge National Laboratory (ORNL) with a collection time between 2 h to 4 h per sample.[23] Samples were loaded in a fused silica capillary, and an empty capillary was collected and subtracted as background.

The average structure of BCSTO was determined through the analysis of diffraction patterns from the NOMAD experiment over a d-space range of approximately 0.15 Å to 6.0 Å (banks 2, 3, and 4). Due to the subtle nature of the phase transition in SSTO, additional high-Q resolution diffraction data was collected at 300 K and 100 K on the POWGEN diffractometer at the SNS at
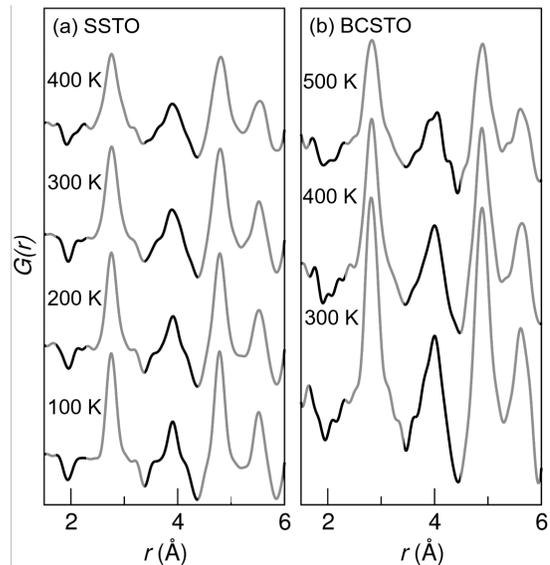

FIG. 1. PDF data of (a) SSTO and (b) BCSTO as a function of temperature (temperatures indicated). The clearest changes are found around 2 Å and 4 Å (highlighted with bolded lines), corresponding to Ti–O and A–A/O–O correlations, respectively.

ORNL ($\Delta d/d$ = 0.001–0.016 for POWGEN vs. $\Delta d/d$ = 0.0036–0.039 for NOMAD) in 6 mm diameter vanadium cans for a collection time of 2 h per sample. The central wavelength of the TOF neutrons was chosen to be 1.066 Å, covering a d-space range of approximately 0.28 Å to 4.60 Å. Analysis of average structures was performed through Rietveld refinement of the neutron diffraction data from both diffractometers using the GSAS software suite with the EXPGUI interface.[24,25]

In order to study the local correlations of the materials, the pair distribution function (PDF), $G(r)$, was obtained by the transformation of the normalized total scattering function, $S(Q)$, collected on NOMAD according to the equation:

$$g(r) - 1 = \frac{1}{2\pi^2 r \rho \Sigma b^2} \int_{Q_{min}}^{Q_{max}} (S(Q) - 1) Q \sin(Qr) dQ \quad (1)$$

where r is the peak position in Å, ρ is the number density in atoms per Å^3, b is the coherent neutron scattering length of each atom in barns, Q is the magnitude of the scattering vector in Å^{-1}, $G(r) = [g(r) - 1]$, Q_{min} = 0.5 Å, and Q_{max} = 31.5 Å^{-1}. Analysis of the local structures were performed by refinement of the real-space PDFs through the PDFgui program.[26] Crystal structures were visualized using the VESTA suite of programs.[27]

III. RESULTS AND DISCUSSION

A qualitative comparison of the PDFs for both samples as a function of temperature (Fig. 1) reveals trends
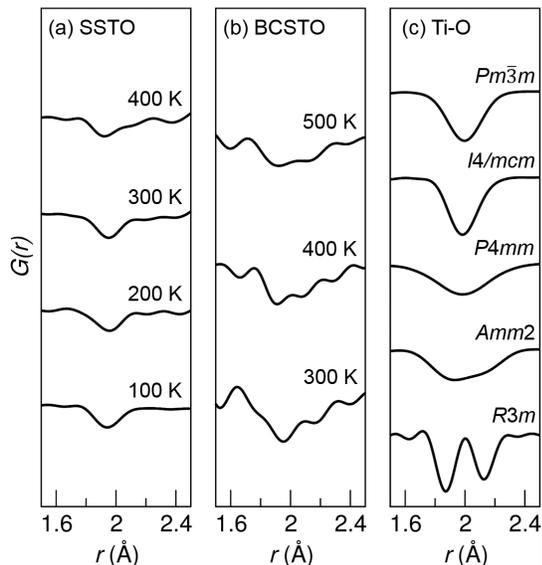
FIG. 2. Experimental and simulated Ti–O nearest neighbor neutron $G(r)$ for (a) SSTO and (b) BCSTO as compared to (c) calculated neutron $G(r)$ from the average structures of $BaTiO_3$ in space groups $Pm\bar{3}m$, $P4mm$, $Amm2$ and $R3m$ from Kwei *et al.*[28] and the $I4/mcm$ average structure phase of $SrTiO_3$.[29] In BCSTO, the Ti–O distribution is resolved into two components at 500 and 400 K. The number of components is less clear at 300 K. An asymmetry of the first Ti–O distribution is observed in the 400 K data of SSTO, with the peak becoming more symmetric upon cooling.

in local correlations upon cooling. All peaks over the 10 Å range show typical behavior of a decrease in peak width and an increase in intensity due to decreased thermal motion at lower temperatures. In the low-r range (less than 5 Å) it is observed that there are two notable areas of change upon cooling: around 2 Å (Fig. 1a) and around 4 Å (Fig. 1b). The correlations around 2 Å are due solely to Ti–O bond interactions in the TiO_6 octahedra, which are negative due to the negative neutron scattering length cross section b of Ti, whereas the correlations around 4 Å are due to both O–O and A–A interactions. From qualitative observations of the resolved Ti–O peaks around 2 Å, it appears in both samples that the first-coordination environment is composed of multiple peaks in the high-temperature phase of each sample. Indeed, two peaks are clearly observed at 500 K in BCSTO, and the number of peaks becomes ambiguous upon cooling of this sample. In SSTO, a definite peak asymmetry is observed at 400 K, and the peak becomes more symmetric as the sample is cooled to 100 K.

A comparison of the observed Ti–O correlations with Ti–O partials calculated from the reported average structure phase transitions in $BaTiO_3$ (Fig. 2) illustrates that a narrow distribution of Ti–O correlations/bond lengths is found in the higher-temperature phases with space group symmetries $Pm\bar{3}m$, $I4/mcm$, and $P4mm$, while multiple resolved Ti–O correlations/bond lengths are ob-

served in $BaTiO_3$ upon transition to the low-temperature phases with symmetries $Amm2$ and $R3m$.[19,28] The trends in the PDFs upon cooling of the Sn^{2+}-substituted samples addresses the primary and unexpected finding of this work: the local TiO_6 octahedra of these Sn^{2+}-substituted titanate perovskites appear to posses a lower symmetry in the high-temperature cubic phase, and become more regular upon cooling.

A. $Sr_{0.9}Sn_{0.1}TiO_3$

Unsubstituted $SrTiO_3$ is a prototypical incipient ferroelectric exhibiting a quantum paraelectric state at low temperatures.[7] Characterized in the cubic $Pm\bar{3}m$ space group at high temperatures, the material undergoes an octahedral rotation resulting in a displacive phase transition to tetragonal $I4/mcm$ at approximately 105 K. This transition has been studied through neutron total scattering techniques and Reverse Monte Carlo (RMC) modeling, and it was determined that the local structure of $SrTiO_3$ possesses very little structural disorder in agreement with the long-range order observed in the material.[30] Upon cooling, $SrTiO_3$ displays a softening of a long wavelength transverse optic (TO) phonon mode, but even upon approaching 0 K, the mode persists, and a true ferroelectric state has yet to be experimentally realized. This persisting paraelectric state is due to a stabilization of the tetragonal phase by quantum fluctuations, which makes the transitions in this system highly sensitive to external influences.[7] For example, compositional substitution creates structural disorder and subsequent local dipolar interactions, such as Ca-induced polar nanoregions in Ca^{2+}-substituted $SrTiO_3$, which prompts a relaxor behavior in the material.[31,32] However, there was no reported evidence of an average structural transition in the Ca^{2+}-substituted material.

The long-range, average structure of SSTO was determined through Rietveld refinement of diffraction data collected on the NOMAD (400 K, 300 K, 200 K, and 100 K) and POWGEN (300 K and 100 K) instruments at SNS. A refined formula of $Sr_{0.94(4)}Sn_{0.06(4)}TiO_3$ was determined from refinement of the 400 K NOMAD data, and used for all other refinements. This data was chosen for the purpose since it covers a larger Q-space range ($Q \approx 1.8\,Å^{-1}$ to $42\,Å^{-1}$ for bank 3 of NOMAD *vs.* $Q \approx 1.4\,Å^{-1}$ to $20\,Å^{-1}$ for bank 2 of POWGEN). This helps avoid excessive correlation of the occupancy with other parameters in the refinement. Previous work by Suzuki *et al.* reported substitution of Sn^{2+} on both the A and B sites of $SrTiO_3$.[8,9] Refinements that modeled this two-site substitution were attempted, but the additional refined occupancies were unstable and the refined model inconclusive. In addition to Sn-substitution on both sites, Sn^{2+} off-centering was reported.[8,9] However, off-centering of an ion in a mixed (alloy) site cannot be refined against Bragg-scattering data, and indeed, this was found to be true insofar as any attempt to do this

TABLE I. Atomic parameters of $Sr_{0.94(4)}Sn_{0.06(4)}TiO_3$ at 300 K, as determined by Rietveld refinement of neutron diffraction data collected on the POWGEN diffractometer. A-site occupancies were determined using the diffraction data collected on the NOMAD diffractometer (wider Q-range of data) and applied to these refinements.

Temperature (K)	300	100
Space group	$Pm\bar{3}m$ (#221)	$P4mm$ (#99)
Cell edge a (Å)	3.9081(5)	3.9000(5)
Cell edge c (Å)	–	3.9068(5)
A U_{iso} (Å^2)	0.0066(5)	0.0031(7)
Ti U_{iso} (Å^2)	0.0040(6)	0.0019(9)
O1 U_{iso} (Å^2)	0.0076(3)	0.005(2)
O2 U_{iso} (Å^2)	–	0.0044(9)
Ti z position	0.5	0.507(2)
O1 z position	–	-0.001(2)
O2 z position	0.5	0.490(2)
R_{wp} (%)	5.1	5.5

yielded unstable refinements. Sn^{2+} off-centering is supported from a perspective of Bond Valence Sums (BVS), with an Sn^{2+} BVS of 1.16 in the $1a$ Wyckoff site of $Pm\bar{3}m$. This suggests Sn^{2+} is under-bonded in the $1a$ site, and a displacement into the variable $6e$ site would create shorter Sn–O bonds and help satisfy the valence of Sn^{2+}. The higher resolution of the POWGEN data was used in an attempt to distinguish phase transitions between the 300 K and 100 K diffraction data. Refinement of the 300 K data was performed in the cubic space group $Pm\bar{3}m$ with Sr^{2+} and Sn^{2+} in the $1a$ Wyckoff position $(0,0,0)$, Ti^{4+} in $1b$ $(0.5, 0.5, 0.5)$, and O^{2-} in $3c$ $(0, 0.5, 0.5)$ and is summarized in Table I. Lattice parameters are in good agreement with the literature for nominal $Sr_{0.9}Sn_{0.1}TiO_3$,[8] and atomic displacement parameters (ADPs, reported in U_{iso}) indicate minimal site disorder in the long-range structure.

PDF data collected at 400 K was fit over a range of 1.5 Å to 5 Å against four separate models with space groups $Pm\bar{3}m$, $I4/mcm$, $P4mm$, and $Amm2$, illustrated in Fig. 3. The correlations between 2.5 Å and 3 Å are well-described by all models, but only $Amm2$ captures the asymmetric shape of the Ti–O correlation around 2 Å. The asymmetric Ti–O correlation indicates that the TiO_6 octahedra are not regular above room temperature, and this supports previously reported polar nano-regions at room temperature in the material.[8–10]

In $SrTiO_3$, the dominant structural change is a rotation of the octahedra facilitated by a change in the positional parameters of the O atoms from cubic $Pm\bar{3}m$, illustrated in Fig. 4a. This rotation inhibits the off-centering of Ti (Fig. 4b), as is observed in ferroelectric perovskites $BaTiO_3$ and $PbTiO_3$. While the ferroelectric nature of $BaTiO_3$ is primarily due to the Ti off-centering, the ferroelectric behavior of $PbTiO_3$ is a cooperative distortion of the TiO_6 octahedra driven by the stereochemically active pair of 6s electrons bound to Pb^{2+}, additionally supplemented by cooperative Ti off-centering. By introducing a dopant that also possesses a lone pair with potential for stereochemical activity, it can be expected that there would be a competition between the rotational process observed in $SrTiO_3$ and the Ti off-centering mechanism in $PbTiO_3$. The $Amm2$ model allows for distortion of the TiO_6 octahedra through both a displacement of the Ti atom and displacements of the O atoms in two directions. It is therefore proposed that at 400 K, these competing processes are both playing a role in the local structure, and the $Amm2$ model provides the best description of the simultaneous displacements of the Ti and O atoms.

TABLE II. Atomic parameters of SSTO at 100 K obtained from refinements of the PDF data over an r-range of 1.5 Å to 5 Å. Similar R_w values and bond lengths suggest both models are appropriate for the data. Consequently, the model with the fewest refinable parameters, $P4mm$, was chosen as the best description of the local structure.

Space group	$P4mm$ (#99)	$Amm2$ (#38)
A U_{iso} (Å^2)	0.0021(7)	0.002(1)
Ti U_{iso} (Å^2)	0.0027(7)	0.0027(9)
O1 U_{iso} (Å^2)	0.0032(9)	0.003(1)
O2 U_{iso} (Å^2)	0.010(3)	0.009(2)
Ti–O (Å)	1.92(5)	1.91(5)
	1.939(3)	1.924(5)
	2.05(5)	2.03(5)
R_w (%)	2.9	2.8

Rietveld refinements of the POWGEN diffraction data collected at 100 K were conducted against structural models in space groups $Pm\bar{3}m$, $I4/mcm$, $P4mm$, and $Amm2$ and resulted in the best fit to the data with the $P4mm$ model (refinement R_w values of 6.8 %, 6.5 %, 5.5 %, and 13.25 %, respectively) with Sr^{2+} and Sn^{2+} in the $1a$ Wyckoff position $(0, 0, z$; $z = 0)$, Ti^{4+} in $1b$ $(0.5, 0.5, z)$, and O^{2-} in $1b$ $(0.5, 0.5, z)$ and $2c$ $(0.5, 0, z)$. On the local scale (fit range 1 Å to 5 Å), similar results were obtained in space groups $P4mm$ and $Amm2$, summarized in Table II. Due to the close proximity of the refined parameters and R-values, the model with the fewest number of refined parameters, $P4mm$, was chosen as the best description of the local structure at 100 K. This result suggests that the rotational transition observed in unsubstituted $SrTiO_3$ is suppressed upon Sn^{2+}-substitution, and even with small concentrations of Sn^{2+}, the transition to the low temperature phase appears to behave closer to that observed in $PbTiO_3$ rather than $SrTiO_3$. The suppression of the rotational transition, coupled with the tendency of off-centering in Sn^{2+} on the A-site may provide an explanation for the origin of the ferroelectric behavior in Sn-substituted $SrTiO_3$. This
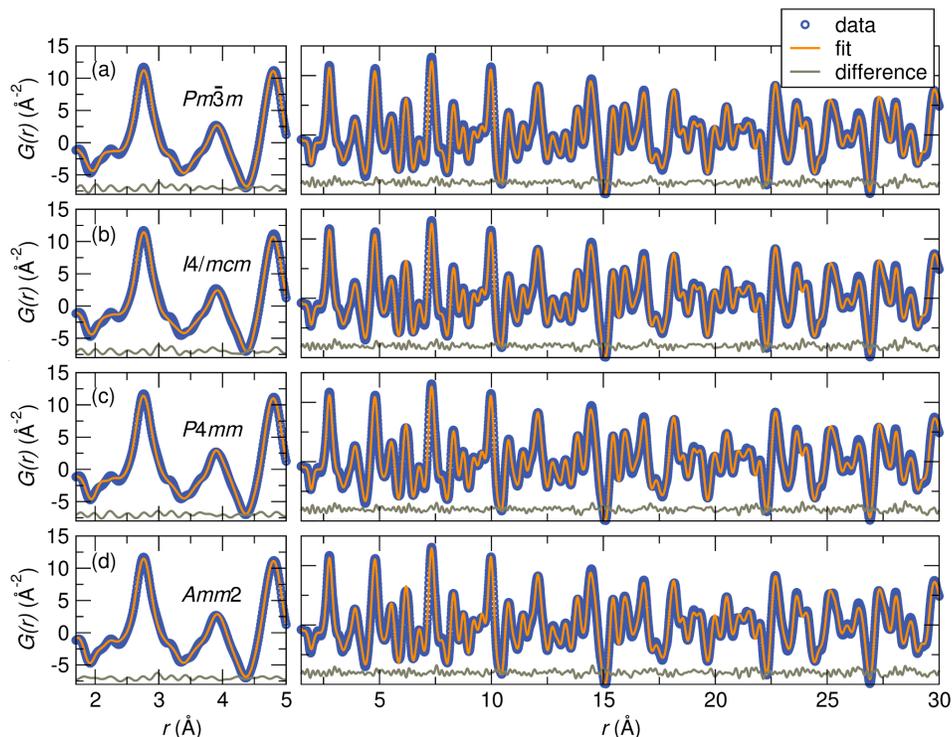
FIG. 3. Fits of the PDF data at 400 K over a range of 1.5 Å to 5 Å and 1.5 Å to 30 Å for SSTO in space groups (a) $Pm\bar{3}m$, (b) $I4/mcm$, (c) $P4mm$, and (d) $Amm2$. Correlations that describe the TiO_6 octahedra around 2 Å are best described by $Amm2$, which accommodates for simultaneous displacements of Ti and O.

highlights the sensitivity of the rotational instability in $SrTiO_3$ and the importance of the active lone pair of 6s electrons to drive this transition.

B. $Ba_{0.79}Ca_{0.16}Sn_{0.05}TiO_3$

The phase transitions in $BaTiO_3$ are well-known and have been studied in detail through neutron total scattering techniques. Globally, $BaTiO_3$ undergoes a cubic ($Pm\bar{3}m$) to tetragonal ($P4mm$) phase transition at approximately 393 K, a tetragonal to orthorhombic ($Amm2$) transition at approximately 278 K, and finally orthorhombic to rhombohedral ($R3m$) transition at approximately 183 K.[28] Analysis of the local structure of $BaTiO_3$ (r-range of 1 Å to 10 Å) revealed that the local structure in the orthorhombic and rhombohedral regimes can be described by the long-range crystallographic phases, but it appears the rhombohedral phase persists above the phase transition temperature, and the phase transition is gradual on a local scale.[19] It was proposed that the orthorhombic to tetragonal phase transition would illustrate a similar and increasingly displacive local phase transition, but modeling of the local structure in various space groups was limited by the resolution of the PDFs and was inconclusive. Furthermore, it was illustrated by Page *et al.* that the local structure of bulk $BaTiO_3$ was better described by the rhombohedral $R3m$

phase at 300 K rather than the global $P4mm$ phase.[33] It has additionally been observed through Extended X-ray Absorption Fine Structure (EXAFS) analysis that locally the TiO_6 are best described as rhombohedral throughout the entire series of average phase transitions, but the correlation length of these octahedra varies with temperature, resulting in an order-disorder series of phase transitions.[34,35]

Ca-substituted $BaTiO_3$ has been explored with various substitution levels, with the maximum solubility limit at $Ba_{0.8}Ca_{0.2}TiO_3$, and is demonstrated to undergo a phase transition from cubic $Pm\bar{3}m$ to the ferroelectric tetragonal $P4mm$ perovskite structure without varying the T_c from that of the parent compound.[13,14] Substitution of Ca^{2+} is accompanied by a linear decrease in the cubic a lattice parameter,[36] which would suggest a depression in the T_c, such as is observed in the $BaTiO_3$–$SrTiO_3$ solid solution.[37] This has been attributed globally to a size mismatch effect of the Ba^{2+} and Ca^{2+} cations.[38] Additionally, analysis of the local structure of $Ba_{0.8}Ca_{0.2}TiO_3$ through RMC modeling of neutron total scattering, XAFS, and diffuse electron scattering indicate simultaneous ferroelectric displacements of the Ca^{2+} and Ti^{4+}, giving rise to the sustained T_c.[39].

Rietveld refinement of the diffraction data from 500 K to 300 K of BCSTO indicates a structural transition from cubic $Pm\bar{3}m$ to tetragonal $P4mm$, and refined parameters are summarized in Table III. Room temperature
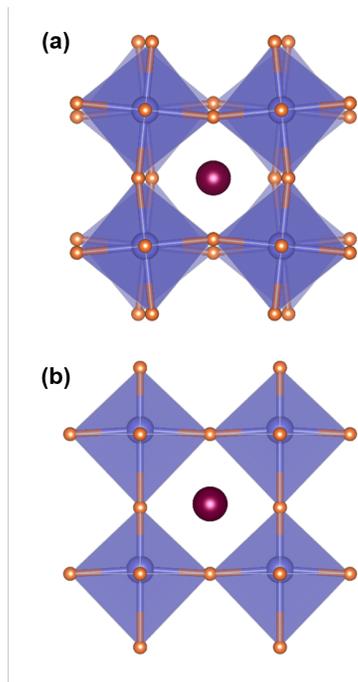
FIG. 4. (a) The structural transition in SrTiO$_3$ from cubic $Pm\bar{3}m$ to tetragonal $I4/mcm$ allows for a positional displacement of O to $(x, y, 0)$ and results in octahedral tilting with no displacement of Ti, whereas (b) the primary displacement of the structural transition in BaTiO$_3$ from $Pm\bar{3}m$ to tetragonal $P4mm$ is in the z direction for the Ti and axial O atoms.
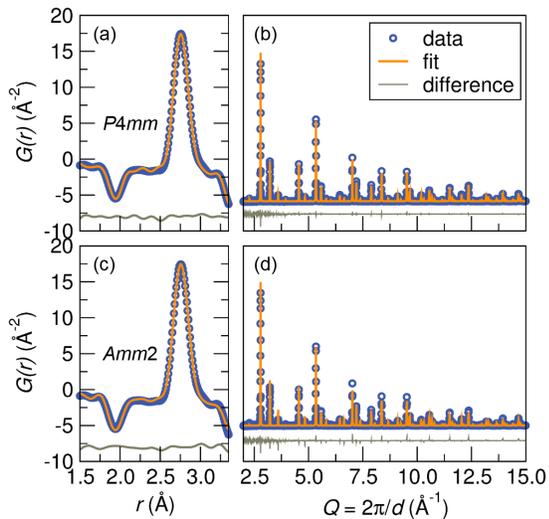

FIG. 5. Refinements of the local and average structure of SSTO at 100 K fit with space groups $P4mm$ [(a) and (b), respectively] and $Amm2$ [(c) and (d) respectively]. The difference curves of each model, shown in gray below, indicate that the $P4mm$ structure provides a better description of the average Bragg scattering than the $Amm2$ structure. Similar fits of the local structure were obtained with both space groups, suggesting that at the local structure level, there is no evidence to support the presence of additional rotational disorder allowed by the lower symmetry structure.

TABLE III. Atomic parameters of BCSTO at various temperatures, as determined by Rietveld refinement of neutron diffraction data collected on the NOMAD instrument. Occupancies were kept at nominal values for the refinement.

Temperature (K)	500	400	300
Space group	$Pm\bar{3}m$ (#221)	$P4mm$ (#99)	$P4mm$ (#99)
Cell edge a (Å)	3.9942(3)	3.9756(5)	3.9765(5)
Cell edge c (Å)	–	4.0035(7)	4.0252(7)
$A\ U_{iso}$ (Å^2)	0.010(1)	0.008(2)	0.005(1)
Ti U_{iso} (Å^2)	0.009(1)	0.012(2)	0.005(1)
O1 U_{iso} (Å^2)	0.011(1)	0.020(3)	0.018(3)
O2 U_{iso} (Å^2)	–	0.008(1)	0.005(1)
Ti z position	0.5	0.482(5)	0.483(7)
O1 z position	–	-0.020(5)	-0.024(5)
O2 z position	0.5	0.503(5)	0.503(7)
R_{wp} (%)	4.9	4.9	6.1

TABLE IV. Atomic parameters of BCSTO at 500 K obtained from refinements of the PDF data over an r-range of 1.5 Å to 5 Å. Employing the $R3m$ model reduces the ADPs of the Ti and O positions and results in more bond lengths with smaller standard deviations, and was therefore chosen as the best description of the local symmetry.

Space group	$Amm2$ (#38)	$R3m$ (#160)
$A\ U_{iso}$ (Å^2)	0.009(3)	0.009(4)
Ti U_{iso} (Å^2)	0.008(5)	0.0059(4)
O1 U_{iso} (Å^2)	0.041(9)	0.009(1)
O2 U_{iso} (Å^2)	0.0016(6)	–
Ti–O (Å)	1.9(1)	1.91(5)
	1.95(2)	1.924(5)
	2.1(1)	2.03(5)
R_w (%)	7.3	9.0

lattice parameters are in good agreement with the literature for the nominal composition.[15,16] Isotropic ADPs of all atoms are relatively high at room temperature, suggesting there is site disorder which deviates from the well-described special positions of the cubic perovskite structure. High ADPs persist for Ti at 400 K, and for the axial oxygens (O1) in the TiO$_6$ octahedra.

Qualitative observations in BCSTO indicate multiple Ti–O bonds resulting in irregular TiO$_6$ octahedra at 500 K, suggesting either $Amm2$ or $R3m$ as appropriate space group descriptions for the local coordination environment of Ti. Fig. 6 show the fits of the PDF data over ranges 1.5 Å to 5 Å and 1.5 Å to 30 Å in space groups models of $Pm\bar{3}m$, $Amm2$, and $R3m$. While a comparison of the R_w values of the $Amm2$ and $R3m$ structures would suggest the local symmetry is better described by $Amm2$, a comparison of the ADPs and bond lengths indicates otherwise (Table IV). When modeled with $R3m$,
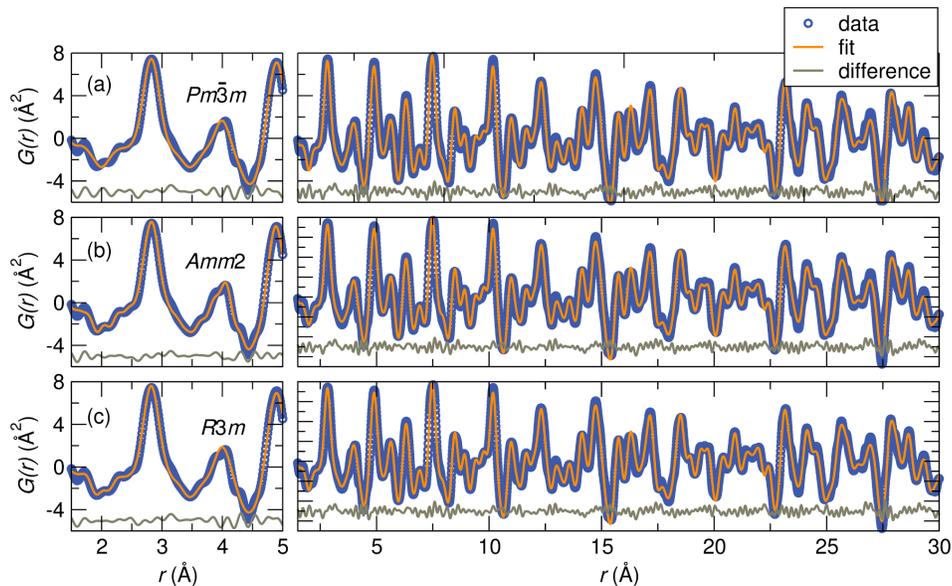
FIG. 6. Fits of the neutron PDF of nominal BCSTO at $500\,\mathrm{K}$ over an r-range of $1.5\,\text{Å}$ to $5\,\text{Å}$ and $1.5\,\text{Å}$ to $30\,\text{Å}$ in space groups (a) $Pm\bar{3}m$, (b) $R3m$, and (c) $Amm2$. Both the $Amm2$ and $R3m$ models capture the multiple Ti–O correlations around $2\,\text{Å}$, but the $Amm2$ model more accurately captures the disorder in the A–A/O–O correlations observed around $4\,\text{Å}$. Similar fits are obtained over an r-range of $1.5\,\text{Å}$ to $30\,\text{Å}$ with the different space groups, supporting the long-range order as best described by cubic $Pm\bar{3}m$.

ADPs and the error associated with the Ti-O bonds are minimized. Additionally, the $R3m$ model uses a smaller number of parameters to model the symmetry, and was therefore chosen as the more accurate description of the local environment at 500 K. While the $R3m$ structure minimizes the Ti and O ADPs, both space groups have relatively high A-site ADPs, which is also reflected in the analysis of the long-range crystallographic structures. This indicates not all of the disorder on the A-site is captured by the proposed space group models. In both crystallographic models, the A atom is located in the center of the large cubic site of the perovskite structure. Once again, BVS calculations can be utilized to rationalize the location of the Sn^{2+} dopant into the $(Ba,Ca)TiO_3$ host lattice. With the refined bond distances at 500 K, a Sn^{2+} BVS of 0.98 is calculated, suggesting the Sn^{2+} is severely under-bonded if located in the $(0,0,0)$ $1a$ Wyckoff site. As with $SrTiO_3$, displacement into the variable $6e$ site would create a few shorter Sn-O bonds and thus raise the valency of the Sn^{2+} atom. Refinements were attempted with this model, but as with SSTO, refinements of the Sn^{2+} position were unstable and inconclusive. As the fitting range of the PDF data is increased, the data begins to approach the long-range, global structure. When the maximum of the fit range of the PDF data is increased to 30 Å, the resulting fits in the three space groups are nearly indistinguishable, supporting the global symmetry observation of a $Pm\bar{3}m$ symmetry from the refinement of the diffraction data.

Based on the results of the local structure at 500 K and the long-range structure at 300 K, the PDF data collected
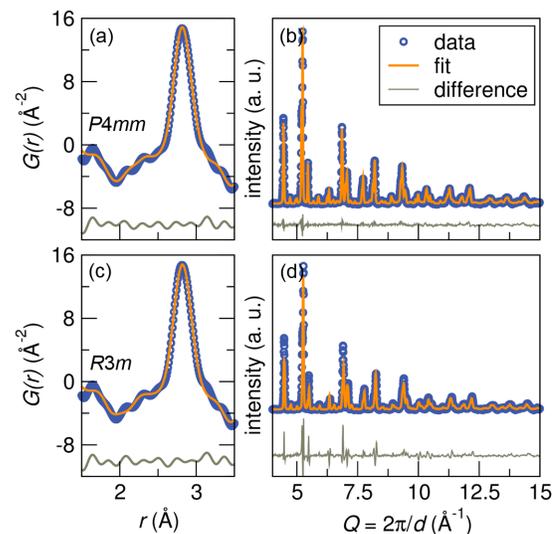

FIG. 7. Refinement of the low-r PDF of nominal BCSTO at $300\,\mathrm{K}$ show similar fits of the Ti–O correlations around $2\,\text{Å}$ with both the $P4mm$ (a) and $R3m$ (b) structural models. Rietveld fits of the neutron data collected on NOMAD indicate that the $P4mm$ model (b) maintains a better description of the average structure than the $R3m$ (d) model.

at 300 K was fit against structural models with space groups $P4mm$ and $R3m$. A comparison of the average and local fits against the two models is illustrated in Fig. 7. It is apparent from the difference curves that $P4mm$ provides a more accurate fit to the diffraction data than $R3m$. However, distinguishing between the fits of the
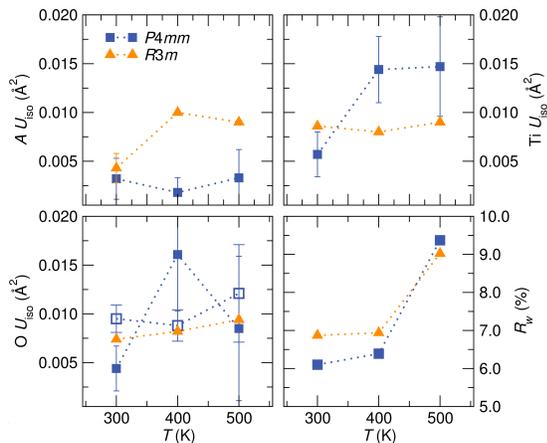
FIG. 8. Isotropic ADPs (U_{iso}) in BCSTO as a function of temperature obtained from various space groups fit against the PDF data over an r-range of 1.5 Å to 5Å. A-site ADPs are minimized in $P4mm$ across the temperature series. ADPs of Ti and O are minimized in the $R3m$ model until 300 K, where the Ti and O1 ADPs (filled symbols) are minimized in $P4mm$. This suggests $R3m$ is a more accurate model at 400 K and 500 K, while $P4mm$ becomes the most accurate description of the local symmetry at 300 K.
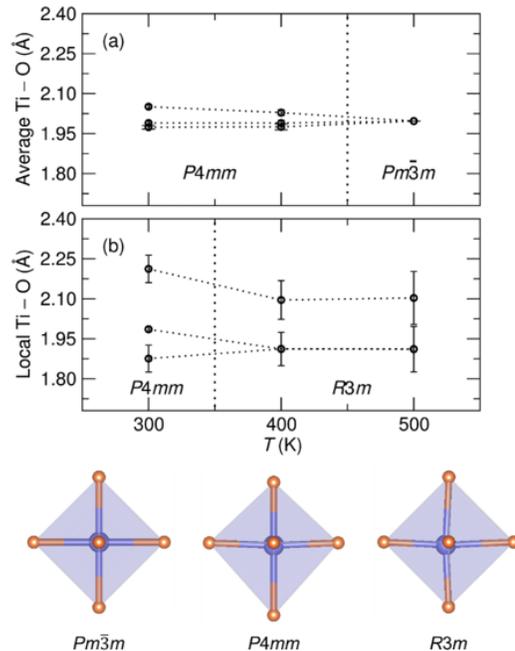

FIG. 9. Ti–O bond lengths in BCSTO of the (a) average and (b) local structure obtained from Rietveld refinement of the NOMAD diffraction data and least-squares refinement of the PDF data, respectively. TiO$_6$ structural units in the $Pm\bar{3}m$, $P4mm$, and $R3m$ structures are shown below the plots.

low-r range of the PDF data is not so straight-forward, and while a smaller R_w results from modeling the local symmetry with $P4mm$ (6.10 % as opposed to 6.34 % in $R3m$) further insight can help distinguish the best model of the local structure. A comparison of the refined ADPs from the two models as a function of temperature over a 1.5 Å to 5 Å fit range (Fig. 8) indicates A-site ADPs are minimized in the $P4mm$ model across the temperature series. Ti ADPs are minimized at 500 and 400 K in the $R3m$ model, while at 300 K ADPs are minimized in the $P4mm$ model. A similar trend is observed in the oxygen ADPs, which have been modeled individually for each crystallographically equivalent site in $P4mm$. Smaller ADPs (and their associated error) indicates which space group best models the local disorder, and therefore at 300 K, the $P4mm$ model is the best description of the local symmetry.

The evolution of the Ti–O bond lengths upon cooling is illustrated in Fig. 9, as well as a pictorial description of the TiO$_6$ octahedra in the $Pm\bar{3}m$, $P4mm$, and $R3m$ structures using the refined values for the average ($Pm\bar{3}m$) and local ($P4mm$ and $R3m$) structures. Rietveld refinements of the average structure indicate Ti displaces towards an axial O, resulting in three Ti–O bond lengths (one short, four medium, and one long) at lower temperatures. Local refinements indicate the Ti is displaced towards the face of the octahedra at high temperatures (two Ti–O bond distances, three short and three long), and displacement towards the axial O (three Ti–O bonds) is only locally observed at low temperature. The phase transition of BCSTO proceeds from a distinctly rhomobohedral local structure to a symmetry that is better described by the $P4mm$ model at 300 K.

In PbTiO$_3$, the short Ti-O bond in tetragonal $P4mm$ is stabilized by the covalency of the Pb-O bond.[40] A similar effect may be present in the Sn-substituted BCSTO, and therefore the local structure in the low-temperature phase more closely resembles that of PbTiO$_3$ rather than BaTiO$_3$, which has a average and local structure that is best described by the rhombohedral space group 300 K.[19] This suggests the series of phase transitions in BCSTO is not an order-disorder type transition as is observed in BaTiO$_3$, as the system is locally distorted in a rhombohedral symmetry only in the high-temperature regime. This indicates that at high temperatures, the local structure of BCSTO is a result the size mismatch of Ba^{2+} and Ca^{2+}, but upon cooling, the stereochemical activity of the lone pairs dominates the transition into a local structure that is more similar to the $P4mm$ model. The elevated T_c of BCSTO can be attributed to a combined effect of the Ba/Ca size mismatch and the enhanced polarization due to the Sn^{2+}. As with SSTO, the lone-pair active A-site cation is dominating the observed structural behavior.

IV. CONCLUSIONS

Samples of Pb-free ferroelectric perovskites with the nominal compositions Ba$_{0.79}$Ca$_{0.16}$Sn$_{0.05}$TiO$_3$ (BCSTO) and Sr$_{0.9}$Sn$_{0.1}$TiO$_3$ (SSTO) were shown to exhibit a

phase transition from average cubic to average tetragonal symmetry upon cooling. The local structure of SSTO is best described by the $Amm2$ model at room temperature, and tends towards a $P4mm$ model at 100 K. The local structure of BCSTO is best described by the $R3m$ model at high temperatures, but ADPs are minimized in the tetragonal $P4mm$ model at lower temperatures, suggesting this is the more consistent description of the local symmetry upon cooling. Both samples exhibit average and local behavior at low temperatures that more closely resembles $PbTiO_3$ rather than the behavior of the more compositionally similar parent compounds $BaTiO_3$ or $SrTiO_3$. This highlights the influence of the Sn^{2+} $5s^2$ lone pair on the structural behavior, despite the small substitution levels. The influence of the stereochemical lone-pairs overrides various competing structural tendencies in both systems, resulting in the emergence of a ferroelectric transition in SSTO and an elevated T_c in BCSTO. Most surprisingly, both samples exhibit lower apparent local symmetry at higher temperatures than at lower temperatures, which is contrary to the usual expectation. This trend is reminiscent of the so-called emphanitic behavior reported in $PbTe$[41] and $SnTe$,[42] suggesting the need for further study, especially above room temperature.

* glaurita@mrl.ucsb.edu

[1] H. Megaw, *Ferroelectricity in Crystals* (Butler & Tanner Ltd., London, 1957).

[2] J. M. Rondinelli, A. S. Eidelson, and N. A. Spaldin, Phys. Rev. B **79**, 205119 (2009).

[3] U. V. Waghmare, N. A. Spaldin, H. C. Kandpal, and R. Seshadri, Phys. Rev. B **67**, 125111 (2003).

[4] D. J. Payne, R. G. Egdell, A. Walsh, G. W. Watson, J. Guo, P. A. Glans, T. Learmonth, and K. E. Smith, Phys. Rev. Lett. **96**, 157403 (2006).

[5] Y. Uratani, T. Shishidou, and T. Oguchi, Jpn. J. Appl. Phys. **47**, 7735 (2008).

[6] S. F. Matar, I. Baraille, and M. A. Subramanian, Chem. Phys. **355**, 43 (2009).

[7] K. A. Müller and H. Burkard, Phys. Rev. B **19**, 3593 (1979).

[8] S. Suzuki, A. Honda, N. Iwaji, S. Higai, A. Ando, H. Takagi, H. Kasatani, and K. Deguchi, Phys. Rev. B **86**, 060102 (2012).

[9] S. Suzuki, A. Honda, K. Suzuki, S. Higai, A. Ando, K. Niwa, and M. Hasegawa, Jpn. J. Appl. Phys. **52** (2013).

[10] T. Nakano, Y. Mikami, K. Abe, S. Suzuki, K. Akiyama, and A. Ando, Ferroelectrics **464**, 72 (2014).

[11] G. H. Haertling, J. Am. Ceram. Soc. **82**, 797 (1999).

[12] G. Burns, Phys. Rev. B Solid State **10**, 1951 (1974).

[13] T. Mitsui and W. Westphal, Phys. Rev. **124**, 1354 (1961).

[14] D. Fu, M. Itoh, S.-y. Koshihara, T. Kosugi, and S. Tsuneyuki, Phys. Rev. Lett. **100**, 227601 (2008).

[15] S. Suzuki, T. Takeda, A. Ando, T. Oyama, N. Wada, H. Niimi, and H. Takagi, Jpn. J. Appl. Phys. **49**, 09MC04 (2010).

[16] S. Suzuki, T. Takeda, A. Ando, and H. Takagi, Appl. Phys. Lett. **96**, 132903 (2010).

[17] S. Suzuki, A. Honda, S. Higai, A. Ando, N. Wada, and H. Takagi, Jpn. J. Appl. Phys. **50**, 09NC11 (2011).

[18] S. Suzuki, N. Iwaji, A. Honda, S. Higai, N. Wada, A. Ando, and H. Takagi, Jpn. J. Appl. Phys. **51**, 09LC08 (2012).

[19] G. H. Kwei, S. J. L. Billinge, S. W. Cheong, and J. G. Saxton, Ferroelectrics **164**, 57 (1995).

[20] K. Sato, T. Miyanaga, S. Ikeda, and D. Diop, Phys. Scripta **T115**, 359 (2005).

[21] K. Page, T. Kolodiazhnyi, T. Proffen, A. K. Cheetham, and R. Seshadri, Phys. Rev. Lett. **101**, 205502 (2008).

[22] R. Armiento, B. Kozinsky, G. Hautier, M. Fornari, and G. Ceder, Phys. Rev. B **89**, 134103 (2014).

[23] J. Neuefeind, M. Feygenson, J. Carruth, R. Hoffmann, and K. K. Chipley, Nucl. Instruments Methods Phys. **287**, 68 (2012).

[24] A. C. Larson and R. B. Von Dreele, Los Alamos National Laboratory Report LAUR **86**, 748 (2000).

[25] B. H. Toby, J. Appl. Crystallogr. **34**, 210 (2001).

[26] C. L. Farrow, P. Juhas, J. W. Liu, D. Bryndin, E. S. Božin, J. Bloch, T. Proffen, and S. J. L. Billinge, J. Phys. Condens. Matter **19**, 335219 (2007).

[27] K. Momma and F. Izumi, J. Appl. Crystallogr. **44**, 1272 (2011).

[28] G. H. Kwei, A. C. Lawson, S. J. L. Billinge, and S. W. Cheong, J. Phys. Chem. **97**, 2368 (1993).

[29] J. M. Kiat and T. Roisnel, J. Phys. Condens. Matter **8**, 3471 (1999).

[30] Q. Hui, M. G. Tucker, M. T. Dove, S. A. Wells, and D. A. Keen, J. Phys. Condens. Matter **17**, S111 (2005).

[31] U. Bianchi, J. Dec, W. Kleemann, and J. Bednorz, Phys. Rev. B **51** (1995).

[32] W. Kleemann, A. Albertini, M. Kuss, and R. Lindner, Ferroelectrics **203**, 57 (1997).

[33] K. Page, T. Proffen, M. Niederberger, and R. Seshadri, Chem. Mater. **22**, 4386 (2010).

[34] B. Ravel, E. Stern, R. Vedrinskii, and V. Kraizman, Ferroelectrics **0193**, 1 (1998).

[35] S. A. T. Redfern, Rev. Mineral. Geochemistry **39**, 105 (2000).

[36] C. Moriyoshi, S. Takeda, E. Magome, Y. Kuroiwa, and J. Ikeda, Jpn. J. Appl. Phys. **52**, 09KF02 (2013).

[37] W. Jackson and W. Reddish, Nature **156**, 717 (1945).

[38] D. Sinclair and J. P. Attfield, Chem. Commun. **16**, 1497 (1999).

[39] I. Levin, V. Krayzman, and J. C. Woicik, Appl. Phys. Lett. **102**, 1 (2013).

[40] R. E. Cohen, Nature **358**, 136 (1992).

[41] E. S. Božin, C. D. Malliakas, P. Souvatzis, T. Proffen, N. A. Spaldin, M. G. Kanatzidis, and S. J. L. Billinge, Science

330, 1660 (2010).

[42] K. R. Knox, E. S. Bozin, C. D. Malliakas, M. G. Kanatzidis, and S. J. L. Billinge, Phys. Rev. B - Condens. Matter Mater. Phys. **89**, 014102 (2014).